Boron Nanosheets for Efficient All-Optical Modulation and Logic Operation

Qiangbing Guo,* Kan Wu, Zhengpeng Shao, Endale T. Basore, Peng Jiang, and Jianrong Qiu*

Due to its unique trivalent electronic configuration, boron features richer properties as well as higher chemical and structural complexities compared with its right neighbor carbon. Consequently, over a decade later than the exfoliation of graphene, borophene has just been experimentally demonstrated on certain metal substrates and under ultrahigh-vacuum conditions, which, however, limit its wide and in-depth experimental researches. Here, for the first time, by employing liquid-exfoliated boron nanosheets, all-optical signal processing application is explored based on its superior photo-thermal response. A stable all-optical modulator is presented, which shows significantly faster response speed and higher modulation efficiency compared with other 2D materials-based similar devices. Furthermore, boron nanosheets-based all-optical logic gating operations are also demonstrated. This work not only presents an excellent 2D material-based all-optical signal processing device, but also marks a significant step toward optical and photonic researches as well as device applications of 2D boron.

The successful exfoliation of graphite into 2D form graphene and resulting remarkable and exotic properties have led to a new field of 2D materials.[1–3] Since then, tons of attention has been focused on the unique properties of materials at their 2D limit. Different kinds of 2D materials beyond graphene, such as transition metal dichalcogenides, hexagonal boron nitride, and black phosphorus (BP), have been discovered and surprised the communities of physicists, chemists as well as material scientists with more distinctive features and new technological opportunities.[2–7]

Dr. Q. B. Guo, E. T. Basore, P. Jiang, Prof. J. R. Qiu
State Key Laboratory of Modern Optical Instrumentation
College of Optical Science and Engineering
Zhejiang University
Hangzhou 310027, China
E-mail: qbguo@zju.edu.cn; qjr@zju.edu.cn
Prof. K. Wu, Z. P. Shao
State Key Laboratory of Advanced Optical Communication
Systems and Networks
Department of Electronic Engineering
Shanghai Jiao Tong University
Shanghai 200240, China

The ORCID identification number(s) for the author(s) of this article can be found under https://doi.org/10.1002/adom.201900322.

As the left neighbor of carbon in the periodic table, boron is very similar to carbon in electronic properties and strong bonding characters, and both undertake important roles in living organisms.[8–11] However, due to the unique trivalent electronic configuration, boron is among the most chemically versatile elements, which shows polymorphism in low-dimensional structures and thus richer properties, such as high-temperature superconductivity, high carrier mobility, massless Dirac fermions, superhardness, to name a few.[12–21] Although the 2D form borophene has recently been experimentally realized by several groups under ultrahigh-vacuum conditions and by another one with chemical vapor deposition (CVD),[12,15,22,23] the related researches of borophene are still mainly concentrated on theoretical predictions and computational calculations.[13,20,21,24–28] Experimental work is largely lagged behind, which, to a large extent, is due to its chemical and structural complexities and thus challenging synthesis.[13,14]

On the other hand, up to now, most of 2D boron-related researches are on the electronic and mechanical properties by theoretical methods, let alone experimental study of its optical properties and related applications. According to several recent theoretical predictions, 2D boron bears fascinating features that are totally different from other 2D materials, such as thickness-dependent transparency and visible/near-infrared plasmons.[26,27] Here, based on liquid-exfoliated boron nanosheets, for the first time, we demonstrate an all-optical phase shifter at the telecommunication band that is mediated by the efficient photo-thermal response in boron nanosheets. The constructed phase shifter shows an order of magnitude faster response speed and higher modulation efficiency compared with other 2D material-based similar devices. Consequently, a high-efficiency and stable all-fiber, all-optical modulator was successfully realized based on a Mach–Zehnder interferometer (MZI) configuration, which could be further employed for all-optical logic gating operations. As proof-of-concept demonstrations, we successfully achieved all-optical logic AND and NOT gates by exploiting the superior photo-thermal response in boron nanosheets. Our work marks an important step toward exploring the optical and photonic applications of 2D boron nanosheets.
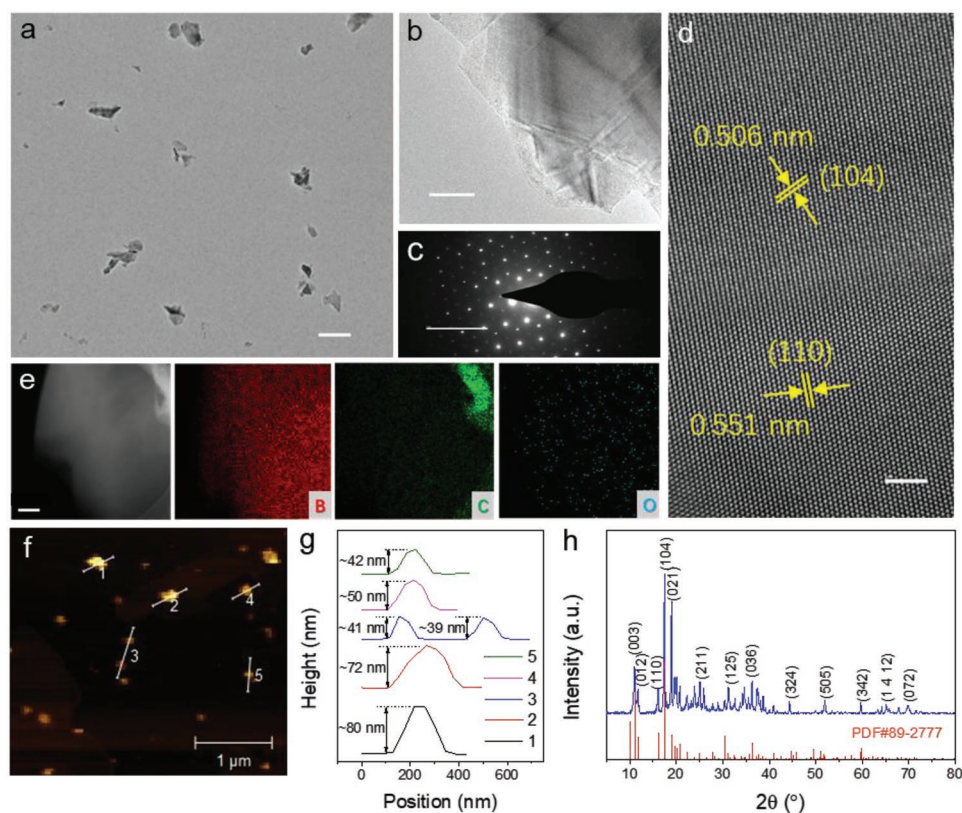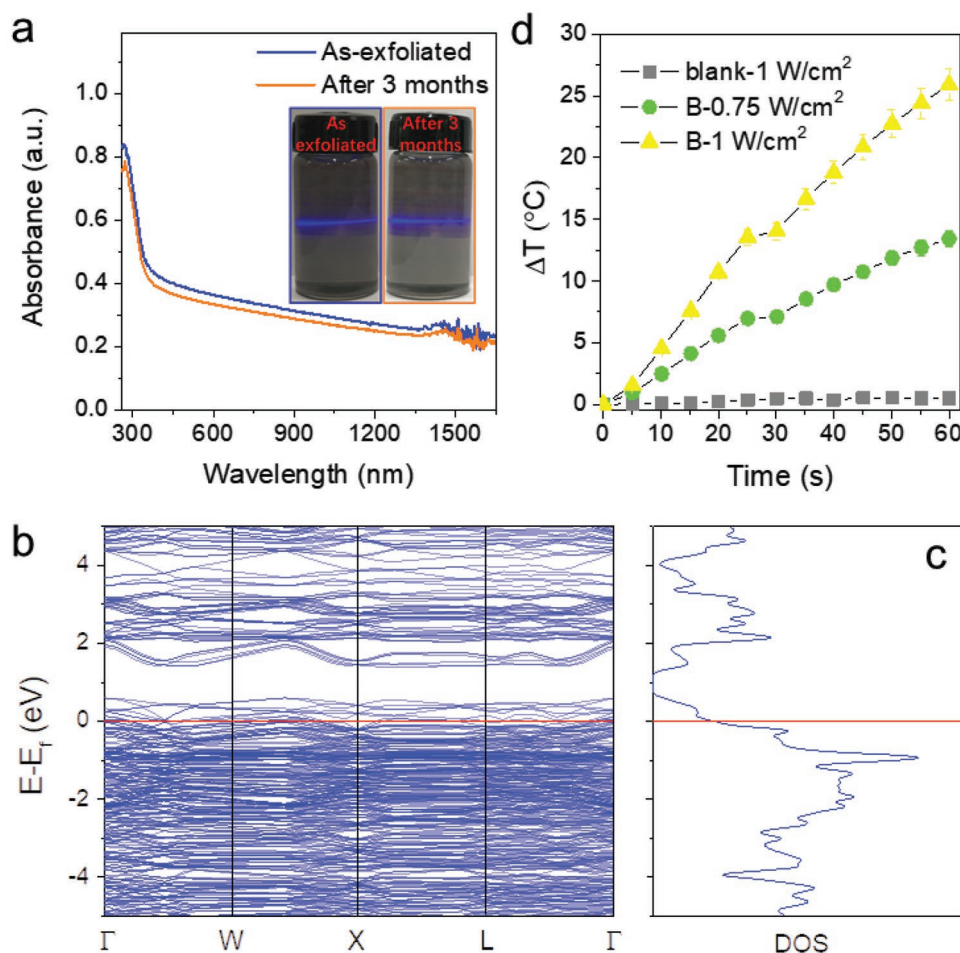
Figure 1. Characterizations of liquid-exfoliated boron nanosheets. a) Typical TEM image of exfoliated boron nanosheets. Scale bar, 200 nm. b) Enlarged image of one nanosheet. Scale bar, 20 nm. c) Typical electron diffraction pattern of nanosheet in (b). Scale bar, 5 1 nm⁻¹. d) HRTEM pattern of nanosheet in (b). Scale bar, 5 nm. e) Elemental mapping images of boron nanosheet, indicating the uniform distribution of boron element throughout the whole sheet while the carbon element could be mainly referred to the supporting substrate (green area). Scale bar, 20 nm. f) Representative AFM topographic image and g) the corresponding height profiles. Scale bar in f), 1 μm. h) XRD pattern of exfoliated nanosheets, which matches well with that of standard phase (β-rhombohedral phase, PDF#89-2777).

Liquid exfoliation has been widely used as a facile and cost-effective method for scalable production of 2D nanosheets, which does not need strict experimental conditions and expensive equipment like molecular beam epitaxy and CVD.[29] Here, sonication-assisted liquid-exfoliation method was employed to exfoliate boron nanosheets in isopropanol alcohol (IPA). The details can be found in the Supporting Information, which is adopted from a previous literature with slight modifications.[30] As shown in **Figure 1**a,b, nanosheets with lateral size ranging from tens to hundreds of nanometers (concentrate in the range of 100–200 nm, also can be confirmed by following atomic force microscope (AFM) characterizations) were obtained, which indicate the exfoliation of bulk boron (size of ≈20 μm). Figure 1e shows the elemental mapping images of a typical nanosheet, demonstrating that it mainly consists of boron element with slight oxidation (O/B ration was estimated to be ≈0.49 at.%). Through X-ray diffraction analysis (Figure 1h), the crystalline phase of exfoliated nanosheets can be indexed to β-rhombohedral boron phase, which can be further confirmed by the electron diffraction pattern (Figure 1c) and high-resolution transmission electron microscope (HRTEM, Figure 1d). Finally, AFM indicates the thickness of exfoliated boron nanosheets concentrates in the range of 40–80 nm, as presented in Figure 1f,g.

Next, we measured the optical absorption property of the exfoliated boron nanosheets. As shown in **Figure 2**a, broadband and featureless absorption ranging from 300 to 1600 nm is observed in boron nanosheet dispersion and the color of the dispersion appears black, which are typical characters of metallic absorption.[31] In order to confirm the metallic nature of boron nanosheets, we calculated the electronic structure and density of state (DOS) by using first-principles density functional theory. The calculation results are shown in Figure 2b,c. Indeed no band gap is observed as evidenced by the nonzero DOSs at the Fermi level, which is in accordance with most previous theoretical predictions and experimental evidences.[12,15,16,24,32] To check the stability of exfoliated nanosheets, we compared the absorption spectra of as-exfoliated dispersion and that of the same dispersion after 3 months. Only slight decrement in absorption intensity is observed (Figure 2a), and the color looks like a little lighter (inset of Figure 2a), which could be attributed to the slight agglomeration as a few black precipitates could be found in the bottom of bottle (further confirmed by X-ray diffraction (XRD)). Therefore, the exfoliated boron nanosheets dispersion is relatively stable in ambient conditions.

To examine light-induced thermal effect in boron nanosheets, we measured photo-thermal heating curves. As presented in Figure 2d, under the same irradiation power of 980 nm laser,

**ADVANCED
SCIENCE NEWS**

www.advancedsciencenews.com

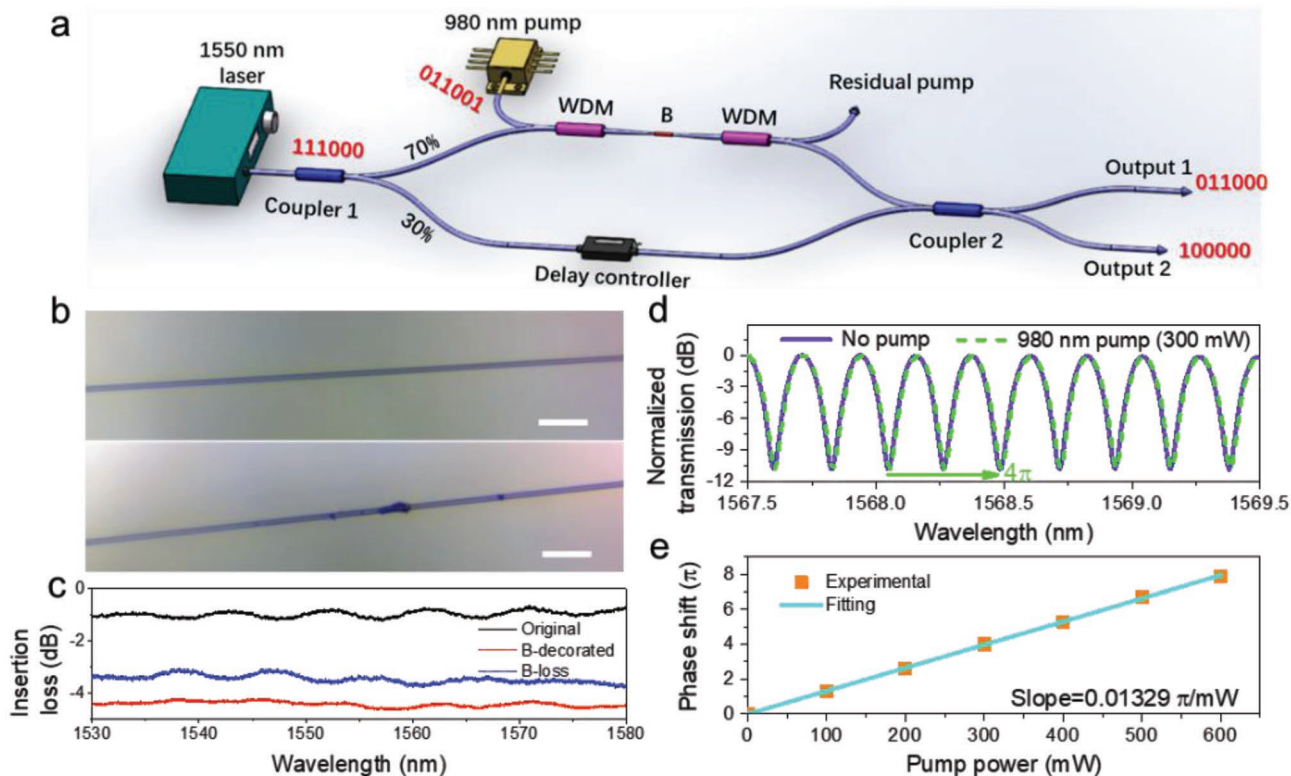**ADVANCED
OPTICAL
MATERIALS**

www.advopticalmat.de

Figure 2. Optical absorption property and electronic structure. a) Absorption spectra of as-exfoliated boron nanosheets in IPA and the same solution after 3 months. The fluctuations around 1500 nm were induced by intrinsic absorption of IPA. Inset shows the corresponding optical images of as-exfoliated (left) and 3 months later (right) dispersions. b) Calculated band structure and c) DOS. The red lines indicate the Fermi level. d) Photo-thermal heating curves of blank IPA and boron nanosheet solution ($\approx$0.1 mg mL^{-1}) under irradiation of 980 nm laser with different power.

the blank IPA shows almost no temperature increment, while obvious temperature increment can be observed in boron nanosheets dispersion. And the higher the irradiation power, the higher the temperature increment, clearly demonstrating efficient photo-thermal effect in boron nanosheets under 980 nm light irradiation.

As for optical modulation, an indispensable technology for modern optical communication, controlling optical properties of a material by changing its refractive index is a widely adopted pathway.[33–44] The refractive index of a material, however, is temperature dependent, which implies a way for optical modulation mediated by thermal control. Therefore, the efficient photo-thermal effect of boron nanosheets could be exploited for optical modulation in an all-optical fashion. On the other hand, due to its simple configuration, low insertion loss/back reflection, and polarization independence, all-fiber structure shows exclusive advantages especially in fiber system.[34,42,44] So here we adopted an all-fiber structure to demonstrate the all-optical modulation. As shown in **Figure 3**a, an all-optical phase shifter, which consists of a boron nanosheets-decorated tapered fiber and a 980 nm pump laser (details can be found in the

Supporting Information), is inserted into one arm (the upper) of an MZI structure to examine the phase shift value. A tapered fiber with diameter of $\approx$10 μm was used, and boron nanosheets were deposited on the surface with a cover length of $\approx$75 μm, as presented by the microscopic images in Figure 3b. The optical loss at around 1550 nm before and after boron nanosheets decoration is shown in Figure 3c, which indicates an $\approx$4.5 dB total loss of the as-prepared phase shifter, with a net loss of $\approx$3.7 dB induced by boron nanosheets and an intrinsic loss of $\approx$0.8 dB by tapered fiber. The small fluctuation of optical loss with wavelength is attributed to the slight diameter fluctuation of tapered fiber used here. By continuously tuning the signal light wavelength from 1567.5 to 1569.5 nm (output of the 1550 nm laser), we can measure the shift of transmission spectrum.

As demonstrated in Figure 3d, when pump the phase shifter with a 980 nm laser at 300 mW, we can observe a 4π phase shift. As the pump power increases, the phase shift increases linearly with a slope efficiency of 0.01329 π mW^{-1} (see Figure 3e), confirming an all-optical phase modulation. The laser-induced phase shift is due to the thermo-optical effect of the tapered fiber because the local temperature increase

**ADVANCED
SCIENCE NEWS**
www.advancedsciencenews.com

**ADVANCED
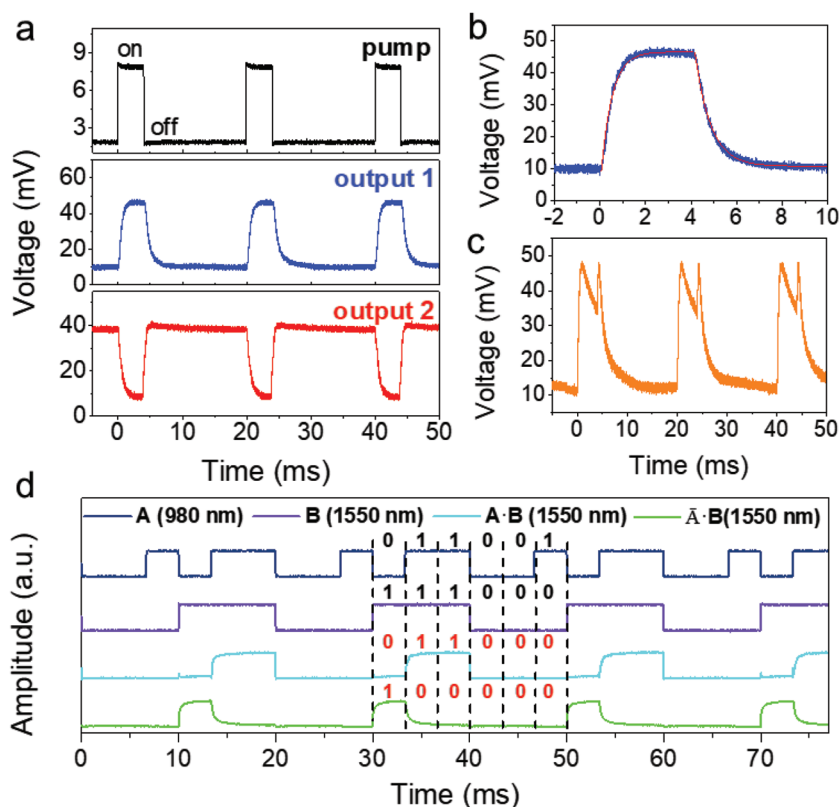OPTICAL
MATERIALS**
www.advopticalmat.de

Figure 3. All-optical phase shifter. a) Schematic illustration of the optical setup, which is based on an MZI configuration. The all-optical phase shifter is embedded into one of the two branches, which consists of two 980/1550 wavelength division multiplexers (WDMs) and a boron nanosheets-decorated tapered fiber in the middle. The whole setup can be used for all-optical modulation with the phase shifter as a controller. b) Optical images of tapered microfiber before (upper panel) and after (bottom panel) deposition of nanosheets. Scale bars, 100 μm. c) Optical loss spectra of original and boron nanosheets-decorated tapered fiber, and the net optical loss by boron nanosheets decoration. d) Normalized transmission spectra of the MZI with no pump (0 phase shift) and 300 mW 980 nm laser pump (corresponding to 4π phase shift), respectively. e) Relationship of phase shift to pump power, which indicates a slope efficiency of 0.01329 π mW^{-1}.

(resulting from the photo-thermal effect in boron nanosheets) brings a change of the refractive index. The phase shift ($\Delta\varnothing$) can be expressed as a function of change in temperature as $\Delta\varnothing = \frac{2\pi}{\lambda_0}\Delta nL = \frac{2\pi}{\lambda_0}\alpha L\Delta T$, where ΔT is the temperature change, α is the thermo-optical coefficient, $\Delta n = \alpha\Delta T$ is the refractive index change, and L is the interaction length of light and boron nanosheets. Therefore, through local thermal control in tapered fiber mediated by photo-thermal effect in boron nanosheets, we can achieve an all-optical phase shifter.

The MZI structure in Figure 3a, with an all-optical phase shifter in one arm, can be used for all-optical modulation.[34,42] According to the output relationship of an MZI device, the output ratio of port 1 is $\eta_{\text{output 1}} = \sin^2(\Delta\varnothing/2)$, while port 2 is $\eta_{\text{output 2}} = \cos^2(\Delta\varnothing/2)$. In consequence, we can modulate the output profiles by controlling the phase difference $\Delta\varnothing$ between the two MZI arms. When a square wave-type modulated laser (980 nm) is used to pump the phase shifter (see upper panel in **Figure 4a**), we can measure output profiles of the signal light (1550 nm) in "output 1" and "output 2" ports, respectively. As shown in Figure 4a, two complementary output profiles can be obtained in the two ports, which change with the pump conditions, demonstrating an all-optical modulation. By fitting the rising and falling edges of a single off-on-off transition in output 1 (Figure 4b, taken from Figure 4a) to exponential

decay functions of $1 - \exp(t/\tau_r)$ and $\exp(-t/\tau_f)$, respectively, the obtained rise and fall time constants are 0.48 and 0.69 ms, which, to our knowledge, are the fastest among 2D materials-based similar devices. As shown in **Table 1**, the rise time constant is about an order of magnitude faster than the others, and the modulation efficiency is also obviously higher. We further tested the bandwidth of the as-built MZI device with a sine wave-type pump (see Figure S1, Supporting Information), which indicates a response time limit of ≈0.41 ms, being well consistent with above results. The superior photo-thermal response might be attributed to the lower mass of boron atom, which, combined with the high stiffness of lattice structure, gives higher electron-phonon coupling and thus higher phonon velocities, implying more efficient thermal transport.[13,20,45] The detailed mechanism, however, deserves further investigations. Besides, when the phase shifter is over driven (corresponding to phase shift over π), the output profile will break into two output peaks with a valley in the middle (Figure 4c), which is similar to that in WS$_2$-based and electro-optical devices.[42] In this case, the rise time constant is also faster than the normal working state, which could be also exploited as a way to further improve the response speed.

Furthermore, the current MZI structure can also be exploited for all-optical logic operations. As a proof-of-concept, an AND

Figure 4. All-optical modulation. a) Modulated pump light profile (980 nm pump in Figure 3a) and corresponding output profiles at output 1 and 2 in the MZI configuration. b) The profile of a single off-on-off transition from output 1 in (a) and exponential fit (red line). c) Output breaking when the MZI is over-driven. d) All-optical AND gate. The waveforms are vertically shifted to provide a clear view.

(poly vinyl alcohol) composite thin film sandwiched between two fibers, we constructed an all-optical NOT gate. In a typical demonstration, when the waveform of 980 nm light is set to periodic "011001" while that of the input signal light (1550 nm) is constant ("111111"), then the output waveform of the signal light is given by "100110," which is the NOT form of that of 980 nm pump light. The device principle is based on the thermal lens effect in the B/PVA thin film. When the boron nanosheets in the thin film absorb the pump light and efficiently generates heat due to photo-thermal response, the refractive index of the thin film on the propagation pathway is changed (thermo-optical effect), which, in turn, induces a local focusing effect in the thin film and the resulting coupling out efficiency is modified. The higher the pump power, the lower the coupling out efficiency (lower output), thus operating as a NOT gate with respect to the 980 nm pump light.

In summary, for the first time, we have exploited liquid-exfoliated boron nanosheets for all-optical signal processing that is mediated by its superior photo-thermal response. The as-constructed all-optical modulator shows significantly faster response speed and higher modulation efficiency compared with other 2D materials-based similar type devices. As the rapid development of big-data approach-based artificial intelligence technology is inducing an extremely fast scaling of data processing and network connections, the device developed here, with easy fabrication, low cost, low power consumption,

gate was demonstrated. As shown in Figure 3a, when the waveform of 980 and 1550 nm light is set to periodic "011001" and "111000," respectively, where "1" represents high power and "0" represents low power. The output 1 of the structure is high only if both 980 and 1550 nm light have a high-level incident power, otherwise, the output is low (close to zero power), indicating an all-optical logic AND operation. In other word, if the waveforms of 980 and 1550 nm light are denoted as A (= "011001") and B (= "111000"), respectively, the output 1 of our system is given by $A \cdot B$ (= "011000") and the output 2 is given by $\bar{A} \cdot B$ (= "100000") where $\bar{A}$ is the inverse of A.

Another important all-optical logic operation, NOT gate, can also be explored based on the superior photo-thermal response in boron nanosheets. As shown in **Figure 5**a, with a B/PVA
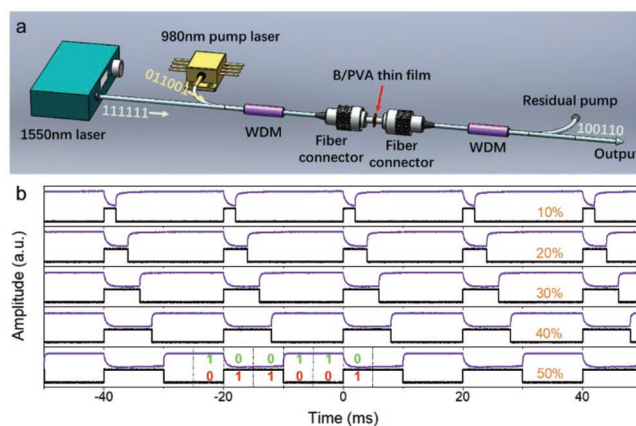
Table 1. Comparison of different 2D materials-based similar devices.

Type	Graphene[34]	WS$_2$[42]	BP[37]	Boron nanosheet
Interaction length [µm]	5000	500	80	75
Loss@1550 nm [dB]	5.4	3.5	10	4.5
Loss@980 nm [dB]	2.1	5	–	2
Modulation efficiency [π mW^{-1} mm^{-1}]	0.018	0.035	0.36	0.17
Rise/fall time constant [ms]	4/1.4	7.3/3.5	2.5/2.1	0.48/0.69

Figure 5. All-optical NOT gate. a) Optical setup. A composite PVA thin film of boron nanosheets (B/PVA) is sandwiched between two fiber connectors. A 1550 nm laser, coupled with a 980 nm pump laser through a WDM, is injected into the B/PVA thin film and the residual 980 nm power is extracted by a second WDM after B/PVA thin film. b) The waveforms of output signal (1550 nm, purple line) and injected pump (980 nm, black line) at different duty cycles.

compact size as well as faster response and higher modulation efficiency, would find great potential in optical interconnection, routing, and gating.[36,39,42] Besides, our work also demonstrates a remarkable step toward optical and photonic applications of 2D boron, of which the research, especially the experimental aspect, is still in its infancy. Considering its exclusive optical properties, like visible/near-infrared plasmons, there is much to expect with respect to the photonic and optical applications as well as novel device concepts of 2D boron nanosheets.[13,27]

Supporting Information

Supporting Information is available from the Wiley Online Library or from the author.

Conflict of Interest

The authors declare no conflict of interest.

[1] K. S. Novoselov, A. K. Geim, S. V. Morozov, D. Jiang, Y. Zhang, S. V. Dubonos, I. V. Grigorieva, A. A. Firsov, *Science* **2004**, *306*, 666.

[2] A. C. Ferrari, F. Bonaccorso, V. Fal'ko, K. S. Novoselov, S. Roche, P. Boggild, S. Borini, F. H. L. Koppens, V. Palermo, N. Pugno, J. A. Garrido, R. Sordan, A. Bianco, L. Ballerini, M. Prato, E. Lidorikis, J. Kivioja, C. Marinelli, T. Ryhanen, A. Morpurgo, J. N. Coleman, V. Nicolosi, L. Colombo, A. Fert, M. Garcia-Hernandez, A. Bachtold, G. F. Schneider, F. Guinea, C. Dekker, M. Barbone, Z. P. Sun, C. Galiotis, A. N. Grigorenko, G. Konstantatos, A. Kis, M. Katsnelson, L. Vandersypen, A. Loiseau, V. Morandi, D. Neumaier, E. Treossi, V. Pellegrini, M. Polini, A. Tredicucci, G. M. Williams, B. H. Hong, J. H. Ahn, J. M. Kim, H. Zirath, B. J. van Wees, H. van der Zant, L. Occhipinti, A. Di Matteo, I. A. Kinloch, T. Seyller, E. Quesnel, X. L. Feng, K. Teo,

N. Rupesinghe, P. Hakonen, S. R. T. Neil, Q. Tannock, T. Lofwander, J. Kinaret, *Nanoscale* **2015**, *7*, 4598.

[3] N. Mounet, M. Gibertini, P. Schwaller, D. Campi, A. Merkys, A. Marrazzo, T. Sohier, I. E. Castelli, A. Cepellotti, G. Pizzi, N. Marzari, *Nat. Nanotechnol.* **2018**, *13*, 246.

[4] J. Y. Wang, S. B. Deng, Z. F. Liu, Z. R. Liu, *Natl. Sci. Rev.* **2015**, *2*, 22.

[5] S. Z. Butler, S. M. Hollen, L. Y. Cao, Y. Cui, J. A. Gupta, H. R. Gutierrez, T. F. Heinz, S. S. Hong, J. X. Huang, A. F. Ismach, E. Johnston-Halperin, M. Kuno, V. V. Plashnitsa, R. D. Robinson, R. S. Ruoff, S. Salahuddin, J. Shan, L. Shi, M. G. Spencer, M. Terrones, W. Windl, J. E. Goldberger, *ACS Nano* **2013**, *7*, 2898.

[6] M. S. Xu, T. Liang, M. M. Shi, H. Z. Chen, *Chem. Rev.* **2013**, *113*, 3766.

[7] K. K. Kim, H. S. Lee, Y. H. Lee, *Chem. Soc. Rev.* **2018**, *47*, 6342.

[8] Z. H. Zhang, E. S. Penev, B. I. Yakobson, *Nat. Chem.* **2016**, *8*, 525.

[9] A. Lopez-Bezanilla, P. B. Littlewood, *Phys. Rev. B* **2016**, *93*, 241405.

[10] X. K. Kong, Q. C. Liu, C. L. Zhang, Z. M. Peng, Q. W. Chen, *Chem. Soc. Rev.* **2017**, *46*, 2127.

[11] Z. H. Zhang, E. S. Penev, B. I. Yakobson, *Chem. Soc. Rev.* **2017**, *46*, 6746.

[12] A. J. Mannix, X. F. Zhou, B. Kiraly, J. D. Wood, D. Alducin, B. D. Myers, X. L. Liu, B. L. Fisher, U. Santiago, J. R. Guest, M. J. Yacaman, A. Ponce, A. R. Oganov, M. C. Hersam, N. P. Guisinger, *Science* **2015**, *350*, 1513.

[13] A. J. Mannix, Z. H. Zhang, N. P. Guisinger, B. I. Yakobson, M. C. Hersam, *Nat. Nanotechnol.* **2018**, *13*, 444.

[14] A. J. Mannix, B. Kiraly, M. C. Hersam, N. P. Guisinger, *Nat. Rev. Chem.* **2017**, *1*, 0014.

[15] B. J. Feng, J. Zhang, Q. Zhong, W. B. Li, S. Li, H. Li, P. Cheng, S. Meng, L. Chen, K. H. Wu, *Nat. Chem.* **2016**, *8*, 563.

[16] J. E. Padilha, R. H. Miwa, A. Fazzio, *Phys. Chem. Chem. Phys.* **2016**, *18*, 25491.

[17] B. J. Feng, O. Sugino, R. Y. Liu, J. Zhang, R. Yukawa, M. Kawamura, T. Iimori, H. Kim, Y. Hasegawa, H. Li, L. Chen, K. H. Wu, H. Kumigashira, F. Komori, T. C. Chiang, S. Meng, I. Matsuda, *Phys. Rev. Lett.* **2017**, *118*, 096401.

[18] G. P. Campbell, A. J. Mannix, J. D. Emery, T. L. Lee, N. P. Guisinger, M. C. Hersam, M. J. Bedzyk, *Nano Lett.* **2018**, *18*, 2816.

[19] X. L. Liu, Z. H. Zhang, L. Q. Wang, B. I. Yakobson, M. C. Hersam, *Nat. Mater.* **2018**, *17*, 783.

[20] T. Tsafack, B. I. Yakobson, *Phys. Rev. B* **2016**, *93*, 165434.

[21] B. Mortazavi, O. Rahaman, A. Dianat, T. Rabczuk, *Phys. Chem. Chem. Phys.* **2016**, *18*, 27405.

[22] R. T. Wu, I. Drozdov, S. Eltinge, P. Zahl, S. Ismail-Beigi, I. Božović, A. Gozar, *Nat. Nanotechnol.* **2019**, *14*, 44.

[23] G. A. Tai, T. S. Hu, Y. G. Zhou, X. F. Wang, J. Z. Kong, T. Zeng, Y. C. You, Q. Wang, *Angew. Chem., Int. Ed.* **2015**, *54*, 15473.

[24] B. Peng, H. Zhang, H. Z. Shao, Y. F. Xu, R. J. Zhang, H. Y. Zhu, *J. Mater. Chem. C* **2016**, *4*, 3592.

[25] H. R. Jiang, Z. H. Lu, M. C. Wu, F. Ciucci, T. S. Zhao, *Nano Energy* **2016**, *23*, 97.

[26] L. Adamska, S. Sadasivam, J. J. Foley, P. Darancet, S. Sharifzadeh, *J. Phys. Chem. C* **2018**, *122*, 4037.

[27] C. Lian, S.-Q. Hu, J. Zhang, C. Cheng, Z. Yuan, S. W. Gao, S. Meng, *arXiv*:1803.01604, **2018**.

[28] X. J. Wu, J. Dai, Y. Zhao, Z. W. Zhuo, J. L. Yang, X. C. Zeng, *ACS Nano* **2012**, *6*, 7443.

[29] X. K. Cai, Y. T. Luo, B. Liu, H. M. Cheng, *Chem. Soc. Rev.* **2018**, *47*, 6224.

[30] H. L. Li, L. Jing, W. W. Liu, J. J. Lin, R. Y. Tay, S. H. Tsang, E. H. T. Teo, *ACS Nano* **2018**, *12*, 1262.

[31] Z. Y. Lin, Y. Liu, U. Halim, M. N. Ding, Y. Y. Liu, Y. L. Wang, C. C. Jia, P. Chen, X. D. Duan, C. Wang, F. Song, M. F. Li, C. Z. Wan, Y. Huang, X. F. Duan, *Nature* **2018**, *562*, 254.

[32] B. J. Feng, J. Zhang, R. Y. Liu, T. Iimori, C. Lian, H. Li, L. Chen, K. H. Wu, S. Meng, F. Komori, I. Matsuda, *Phys. Rev. B* **2016**, *94*, 041408.

[33] Q. B. Guo, Y. H. Yao, Z.-C. Luo, Z. P. Qin, G. Q. Xie, M. Liu, J. Kang, S. A. Zhang, G. Bi, X. F. Liu, J. R. Qiu, *ACS Nano* **2016**, *10*, 9463.

[34] X. T. Gan, C. Y. Zhao, Y. D. Wang, D. Mao, L. Fang, L. Han, J. L. Zhao, *Optica* **2015**, *2*, 468.

[35] L. H. Yu, Y. L. Yin, Y. C. Shi, D. X. Dai, S. L. He, *Optica* **2016**, *3*, 159.

[36] Z. P. Sun, A. Martinez, F. Wang, *Nat. Photonics* **2016**, *10*, 227.

[37] Y. Z. Wang, F. Zhang, X. Tang, X. Chen, Y. X. Chen, W. C. Huang, Z. M. Liang, L. M. Wu, Y. Q. Ge, Y. F. Song, J. Liu, D. Zhang, J. Q. Li, H. Zhang, *Laser Photonics Rev.* **2018**, *12*, 1800016.

[38] Q. B. Guo, Z. P. Qin, Z. Wang, Y.-X. Weng, X. F. Liu, G. Q. Xie, J. R. Qiu, *ACS Nano* **2018**, *12*, 12770.

[39] G. T. Reed, G. Mashanovich, F. Y. Gardes, D. J. Thomson, *Nat. Photonics* **2010**, *4*, 518.

[40] S. Gan, C. T. Cheng, Y. H. Zhan, B. J. Huang, X. T. Gan, S. J. Li, S. H. Lin, X. F. Li, J. L. Zhao, H. D. Chen, Q. L. Bao, *Nanoscale* **2015**, *7*, 20249.

[41] S. L. Yu, X. Q. Wu, K. R. Chen, B. G. Chen, X. Guo, D. X. Dai, L. M. Tong, W. T. Liu, Y. R. Shen, *Optica* **2016**, *3*, 541.

[42] K. Wu, C. S. Guo, H. Wang, X. Y. Zhang, J. Wang, J. P. Chen, *Opt. Express* **2017**, *25*, 17639.

[43] Q. B. Guo, Y. D. Cui, Y. H. Yao, Y. T. Ye, Y. Yang, X. M. Liu, S. A. Zhang, X. F. Liu, J. R. Qiu, H. Hosono, *Adv. Mater.* **2017**, *29*, 1700754.

[44] K. Wu, Y. F. Wang, C. Y. Qiu, J. P. Chen, *Photonics Res.* **2018**, *6*, C22.

[45] D. F. Li, J. He, G. Q. Ding, Q. Q. Tang, Y. Ying, J. J. He, C. Y. Zhong, Y. Liu, C. B. Feng, Q. L. Sun, H. B. Zhou, P. Zhou, G. Zhang, *Adv. Funct. Mater.* **2018**, *28*, 1801685.